Applied Catalysis B: Environmental 237 (2018) 327–338

Contents lists available at ScienceDirect

Applied Catalysis B: Environmental

journal homepage: www.elsevier.com/locate/apcatb

Copper-nickel catalysts from hydrotalcite precursors: The performance in NO reduction by CO

Daniel Lopes, Fatima Zotin, Luz Amparo Palacio*

Universidade do Estado do Rio de Janeiro, Instituto de Química, Rua São Francisco Xavier, 524, CEP: 20550-900, Rio de Janeiro, RJ, Brazil

ARTICLE INFO

Keywords:
NO reduction
Ni-Cu-Al hydrotalcites
Terephthalate anion
In-situ XANES

ABSTRACT

In the present work, catalysts based on copper and nickel and obtained from hydrotalcite like-compounds were evaluated in the NO reduction by CO in order to analyze the activity and yield to N_2 and N_2O. The co-precipitation method was used to obtain catalyst precursors with variable (y = Cu/(Cu + Ni)) molar ratios values (y = 0, 0.3, 0.5, 0.7 and 1). The use of terephthalate as a compensation anion was a novelty in this series of precursors. The formation of layered compound was observed at y values smaller than or equal to 0.7. The X-ray absorption spectroscopy analysis showed that the Cu-catalysts obtained from the calcination of the precursor at 600 °C have only Cu^{2+} species, and Cu^{+} and Cu° species were found throughout the reaction as observed by in situ XANES. However, even during pretreatment at 500 °C under helium flow, copper reduced species were observed. According to TPR results, the introduction of a second metal decreased the reduction temperature of the monometallic catalysts. An easier reduction of copper oxide over nickel is also clear. Cu content, calcination temperature, compensation anion of the hydrotalcite and a pre-reduction of the catalysts significantly impact on the activity and selectivity of the catalysts.

1. Introduction

The world is constantly changing and the environment is one of the main concerns. The quality of the air and its pollution have been the subject of many studies, and special attention has been given to NO_x emissions. Nitrogen oxides are known to have adverse effects on human health and are also associated with several global effects, for example the increase of smog and acid rain. The sources of nitrogen oxides are mainly anthropogenic, mostly associated to the combustion of fossil fuels.

Selective catalytic reduction of NO by CO is one of the most used reactions for studying NOx abatement from mobile sources (Reaction (1)). A parallel reaction can also produce N_2O (Reaction (2)), a greenhouse gas that is 300 times more harmful than CO_2 in its warming potential. Nitrous oxide can also react with CO to form N_2 (Reaction (3)).

$$NO + CO \rightarrow ½\ N_2 + CO_2 \quad (1)$$

$$2NO + CO \rightarrow N_2O + CO_2 \quad (2)$$

$$N_2O + CO \rightarrow N_2 + CO_2 \quad (3)$$

Catalysts such as those based on transition metals are being studied in order to obtain more active and selective systems, with copper being one of them. Some works with copper-based catalysts attribute the catalytic activity to a redox-type mechanism (Cu^{2+}/Cu^{+}) under reaction conditions [1–3].

Several types of copper-containing catalysts have been used for the reaction of NO with CO, most of them are supported on CeO_2 [3,4], Al_2O_3 [5,6] and mesoporous, such as MCM-41 [7]. Among the bulk catalysts that contain copper in its structure, the perovskites [8] and spinels [9] can be found.

Precursors that could incorporate metals (such as copper) with potential activity in the NO reduction reaction by CO are hydrotalcite-like materials. Hydrotalcites is a class of compounds with lots of applications, including adsorbents, catalysts, among others. They are layered double hydroxide, whose structure is characterized by layers with a brucite-like structure. They have the general formula $M^{2+}_{1-x}N^{3+}_x(OH)_2(A^{-n}).nH_2O$, where M^{2+} and N^{3+} are the divalent and trivalent cations, respectively, and A^{-n} is the interlayer anion [10].

After thermal treatment, hydrotalcites produce oxides (bulk catalyst) with homogenous distribution, where the metals have intimate interactions and unique catalytic activities [11,12]. Usually, oxides obtained from hydrotalcite exhibit intermediate characteristics from the individual oxides [13]. The flexible structure of hydrotalcite like-compounds offers the opportunity to introduce a wide range of metals and anions. The literature reports that various metals may occupy the

* Corresponding author.
E-mail address: lpalacio@uerj.br (L.A. Palacio).

https://doi.org/10.1016/j.apcatb.2018.06.007
Received 30 January 2018; Received in revised form 20 May 2018; Accepted 3 June 2018
Available online 04 June 2018
0926-3373/

sites of divalent atoms, such as Ni, Cu and Zn. Similarly, different anions can be used, such as carbonate, nitrate, borate, among others [14].

There are few articles in the literature which use catalysts obtained from Cu-Al hydrotalcite-type precursors, probably because they are difficult to obtain. The distortion of Cu octahedral, caused by the Jahn-Teller effect, prevents the formation of a defined and pure phase. Only with quite specific synthesis conditions is it possible to form a pure hydrotalcite like-precursor with Cu and Al [15–17]. The formation of malachite (copper hydroxycarbonate) as a segregated phase is common when carbonate is used as the compensation anion [18,19].

In previous studies carried out in our laboratory, Cu-Al catalysts obtained from hydrotalcite type precursors using carbonate as the compensation anion showed high thermal stability and activity in the NO reduction by CO [15,16]. Carbonate is usually present as the intercalated anion located between the layers, due to the hydrotalcite having a high affinity for it. Muñoz et al. [15] studied catalysts obtained from Cu-Al hydrotalcites with carbonate as the compensation anion. According to their results, a pure precursor generates a catalyst with better catalytic performance than those in which a mixture of malachite and hydrotalcite is found. Later, Corrêa et al. [16] analyzed the effect of Cu and Al ratio in the reaction and it was found that the catalyst with the 50:50 Cu:Al produced less N_2O. Mixed oxides obtained from calcination of a hydrotalcite and malachite mixture tend to form a larger amount of N_2O at low temperatures. Also, a physical mixture of Al_2O_3 and CuO did not have the same performance as a catalyst obtained from Cu-Al hydrotalcite [15,16].

In order to avoid the formation of malachite due to the presence of carbonate anion in the Cu-Al hydrotalcite precursors, other compensation anions could be tested. Terephthalate is a promising anion since it presents hydrophobicity and bifunctional character (it can interact with both layers of the hydrotalcite). Hydrotalcites with terephthalate as the compensation anion have a higher interlayer space (c.a. 14.6 Å) in comparison with a carbonate anion (c.a. 7.6 Å) [20].

Among the hydrotalcite like-materials synthesized using terephthalate as the compensation anion, Ni-Al [21], Co-Al [22], Zn-Al [23] and Mg-Al [24] can be found. Cu-Al hydrotalcite materials with terephthalate were not reported in the literature to date. Arias et al. [21] showed that it is possible to obtain an ordered hydrotalcite structure with a Al/(Al + Ni) ratio equal to 0.5 using terephthalate, which is not possible when carbonate is used as the compensation anion. The high stability of the layers with this anion is promising for practical applications. In order to synthesize the Cu-Al-TA (TA: terephthalate) hydrotalcite precursor, a system with a proven purity can be used to systematically incorporate copper such as the Ni-Al-TA. In addition, Ni-Cu catalysts have been used with good results in NO conversion [25,26].

Therefore, this work aims to study catalysts obtained from the calcination of Ni-Cu-Al-TA precursors with hydrotalcite structures and with different Cu/(Ni + Cu) ratios (from 0 to 1). The specific objectives are to compare the catalytic behavior of Cu-Al precursors (free of carbonate) with other copper-aluminum systems in the NO reduction by CO and to evaluate the effect of Ni content, pretreatment atmosphere and calcination temperature in the catalysts performance.

2. Experimental

2.1. Synthesis of the precursors

First of all, five different hydrotalcite-like precursors were prepared. Copper and nickel contents were varied in order to obtain metal ratios y = Cu/(Ni + Cu), were varied around 0, 0.3, 0.5, 0.7 and 1. The procedure was based on the work of Henao et al. [21] for the Ni-Al-TA system. Some modifications were carried out in order to find the best conditions to obtain a carbonate-free product without using an inert atmosphere (N_2) during the synthesis. Al content was established in order to have x = Al/(Ni + Cu + Al) equal to 0.5. Five aqueous solutions (35 ml each) with 0.005 mol of $Al(NO_3)_2{\cdot}9H_2O$ (98% Sigma-Aldrich) and 0.005 mol of Ni + Cu were prepared. $Ni(NO_3)_2{\cdot}6H_2O$ (97% Vetec) and $Cu(NO_3)_2{\cdot}3H_2O$ (99% Vetec) were used as nickel and copper source, respectively. Another aqueous solution (35 ml) containing 0.02 mol of sodium hydroxide (99% Vetec) and 0.005 mol of terephthalic acid (98% Sigma-Aldrich) was used as the precipitating agent and to introduce the compensation anion. Hence, the intended formula was $(Cu_yNi_{1-y})_{0.5}Al_{0.5}(OH)_2(TA)_{0.25}.nH_2O$. The solutions were added simultaneously to a beaker containing 50 mL of distilled water under constant stirring. The pH was controlled at 6.5 using a Provitec model 2900 pH controller. The syntheses were performed at 50 °C under magnetic stirring for 1 h. Then, they were aged for 24 h at room temperature, and after that the solids obtained were filtered, washed with distilled water (1.5 L) and dried at room temperature. The precursors were labeled as Cu-100y (with y from 0 to 1), indicating the percentage of Cu in the total of divalent metals.

2.2. Preparation of the catalysts

The precursors were calcined in a Jung 4240 muffle at 600 °C (or 900 °C) for 4 h with a heating rate of 10 °C min^{-1} in static conditions (air atmosphere) to obtain the catalysts. For the nomenclature of these catalysts a c or t suffix was added to the precursor name in order to identify the calcination temperature used (Cu-100yc for 600 °C and Cu-100yt for 900 °C).

2.3. Characterization of materials

X-ray diffraction (XRD) analysis of the precursors and the catalysts were performed on a Rigaku Ultima IV model equipment with a CuKα source (λ = 0.15406 nm), in the range of 2θ from 5° to 70°, at 40 kV and 20 mA.

XRD patterns of the precursors calcined at 600 °C were obtained using a synchrotron light source (Synchrotron Light Laboratory LNLS, Campinas, Brazil), with a Si (111) monochromator. The patterns were obtained between 25 and 70° in 2θ, with 0.154820 nm wavelength.

For the identification of the crystalline phases, the ICSD (Inorganic Crystal Structure Database) was used. The *a* and *c* cell parameters were calculated using the formulas widely published in the literature for hydrotalcite structure [27], $a = 2d(110)$ and $c = 3d(003)$, where *d* is the interplanar distance. For all catalysts, a Rietveld refinement was performed in order to quantify the crystalline phases; for this, Powdercell and GSAS software were used [28,29]. GSAS is a more robust software, and then it was used in less crystalline samples. The average crystallite size was calculated using the Scherrer equation [30].

Thermogravimetric analysis (TGA) and differential thermal analysis (DTA) were performed, simultaneously, in a SDTQ 600 equipment, under 20 mL min^{-1} of N_2 with a heating rate of 10 °C min^{-1}, from room temperature up to 900 °C. A Perkin Elmer Spectrum One spectrometer was used to perform Fourier-transformed infrared spectroscopy (FTIR). The tablets were prepared using 1%w/w of the catalyst in KBr. The composition of the metals was determined by X-ray fluorescence analysis (XRF), performed on a WDS-1 type AXIOS (Panalytical) spectrometer. Textural properties of the precursors and catalysts (outgassed at 300 °C for 12 h), were obtained from N_2 adsorption isotherms using the BET and BJH methods and a Micromeritics ASAP 2020 apparatus.

Temperature programmed reduction (TPR) was performed using Micromeritics Autochem II Model 2920 equipment. Samples were pretreated by heating from room temperature to 500 °C under argon atmosphere (50 mL min^{-1}) for 1 h. The reduction of the materials was carried out under a flow rate of 50 mL min^{-1} H_2/Ar (10% v/v) and a heating rate of 10 °C min^{-1}, from room temperature to 800 °C.

XANES (X-ray Absorption Near Edge Structure) spectra were measured on the D06A-DXAS beamline of the LNLS storage ring, operated at 1.37 GeV with a maximum beam current of 250 mA.

Monochromatization of the incident beam was done using channel cut Si (111) crystals. The absorption spectra at the Cu K edge were recorded in the transmission mode, in a photon energy range between 8800–9200 eV, using a CCD camera. Spectra were obtained at room temperature for the catalysts treated at 600 °C. To better understand the species involved in the products formation during the reaction, in situ XANES was carried out for one of the catalysts. Thick pellets were formed by dry-pressing the catalyst (from 15 to 27 mg) with 90 mg of binder (boron nitride) and disposed in the reactor that was quite different from the one used in the catalytic test, since it is not a fixed bed. The reactor is a tube where the pellet is arranged in a sample holder, positioned perpendicular to the flow but not necessarily percolated by it.

A pretreatment of the catalyst was done under helium flow (40 mL min^{-1}), and at a heating rate of 10 °C min^{-1} up to 150 °C, for 20 min. The reaction was carried out using a gas mixture consisting of 50 mL min^{-1} 5% NO/He and 50 mL min^{-1} 5% CO/He. The reactor was heated from room temperature to 500 °C, at a rate of 5 °C min^{-1}, with a plateau of 10 min.

The literature has reported the linear combination method to quantify the species through XANES spectra analysis [31,32]. For our in-situ measurements, this method was performed using Polymath software [33]. First, the proportion of the initial (obtained at room temperature) and final (at 500 °C) spectrum for each full range spectrum (from room temperature up to 500 °C) were calculated by linear combination. Next, those two extreme spectra (at room temperature and at 500 °C) were fitted with the experimental reference spectra (Cu^{2+}, Cu^{+} and Cu^{0}) to obtain the copper composition of the sample at those temperatures. Finally, for each spectrum, the fraction of the extreme spectra was multiplied for their composition of Cu species, resulting in the fraction of Cu^{2+}, Cu^{+} and Cu^{0} in the whole temperature range.

2.4. Catalytic tests

The catalytic evaluation was performed using a U-shaped Pyrex reactor (6.6 mm internal diameter), positioned in a vertical furnace equipped with a PID temperature controller. The reaction mixture contained 1% (v/v) NO and 1% (v/v) CO in He. Samples of 0.12–0.13 g of the catalysts were tested at a flow rate of 225 mL min^{-1} (GHSV = 9600 h^{-1}), from room temperature up to 500 °C, with a heating rate of 2 °C min^{-1}. The analysis of the reagents and products were performed in an Agilent 6890 N gas chromatograph equipped with a thermal conductivity detector using a Porapak N column in series with a Molecular Sieve column, both operating isothermally. This configuration allowed the concentration of the reactants (CO and NO) and products (N_2, N_2O and CO_2) to be determined every 7 min. The catalyst bed with controlled particle size (40–60 mesh) was diluted with silicon carbide (mass ratio of 1:3). In all cases, carbon balances is close to 100%, within the experimental accuracy of the system.

A long-term stability study was performed with the most promising catalysts of this study. Catalytic tests similar to the previous ones were carried out. After reaching the desired temperature (300 and 500 °C), the catalyst was maintained under these conditions (under reaction stream flow) for at least 9 h.

3. Results and discussion

3.1. Precursors

According to XRF results (Table 1) the Al/(Al + Ni + Cu) ratio was near the nominal value (0.5). Cu/(Cu + Ni) was also quite similar to the expected values. Thus, in general the trivalent and divalent elements were incorporated in the desired proportion.

The X-ray diffraction of the precursors is shown in Fig. 1. The main Miller index corresponding to hydrotalcite phase with terephthalate anion [21] is marked and an inset plot was added to highlight the two main peaks. A different copper content affects the structure of the solid, as observed. The precursor with 100% nickel (Cu-0) was identified as terephthalate hydrotalcite, where 2θ = 6.22° (003), 12.58° (006), 19.0° (009) and 25.38° (0012) correspond to different orders of the basal space. For hydrotalcite this is indeed the interlayer space, as described for Ni-Al-TA [21]. The first peak in the position 2θ = 6.22° means that the terephthalate is vertically oriented, because its interplanar distance, *d*(003), is 14.2 Å [34]. Other peaks, typical of hydrotalcite-like materials are also present (35.13, 38.62, 45.8 and 62.49°) [10,27].

Table 1
X-ray fluorescence analysis of precursors.

Sample	Composition (%w/w)			Al/(Al + Ni + Cu) molar ratio[a]	Cu/(Ni + Cu) molar ratio[b]
	Al_2O_3	NiO	CuO		
Cu-100	39.3	0	60.7	0.50	1 (1)
Cu-70	41.8	18.6	39.6	0.52	0.67 (0.7)
Cu-50	37.7	34.1	28.2	0.48	0.44 (0.5)
Cu-30	44.9	41.7	13.4	0.55	0.23 (0.3)
Cu-0	38.3	61.7	0	0.48	0 (0)

[a] The nominal value is 0.5.
[b] Between parenthesis is the nominal value.

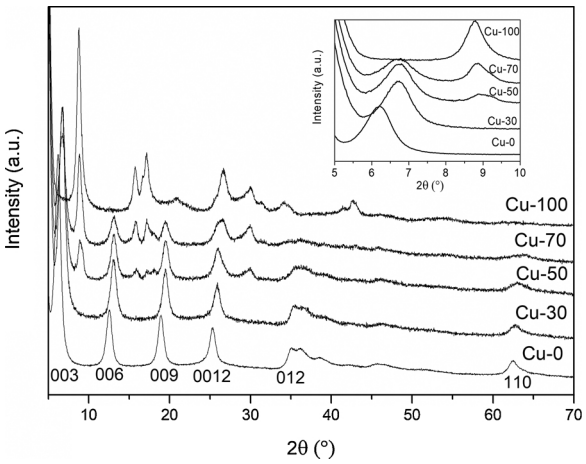

Fig. 1. XRD of the precursors.

Almost the same pattern appears in the sample Cu-30, but for the other precursors, other peaks appear in 8.8, 15.8, 17.2, 20.9, 26.6 and 30.0° (2θ). Seemingly, they belong to a segregate phase, which is the only one present in Cu-100. Then, Cu-50 and Cu-70 are a mixture of two phases. According to the literature, a material (aluminum hydroxyterephthalate - $Al(OH)(C_8O_4H_4)$ [35]) was found to be quite similar in structure to Cu-100. The comparison of its pattern with Cu-100 (see Fig. S1 of the Supplementary Material) shows that there are some shifts in the peaks at 15.2 and 20.9° (2θ), and the peaks in higher angles are more intense for Cu-100. It is possible that some Cu has been incorporated in the structure too, producing an aluminum-copper hydroxyterephthalate, which changes the XRD profile. However, this hypothesis needs to be confirmed by carrying out structural determination studies. As expected, malachite (copper hydroxycarbonate) was not identified in Cu-100, nor in the other crystalline Cu precursors. X-ray diffraction indicate that pure hydrotalcite was obtained for Ni-Cu-Al-TA with 23% of Cu and 100% of Ni, but not for 100% of Cu (percentages relative to total divalent elements). Ni-Cu-Al-TA hydrotalcite type material has not been reported in the literature, being a novelty in this work.

It is noteworthy that the intensity of the peaks of the hydrotalcite phase decreases with the increment of copper, giving place to the phase in Cu-100. A semi-quantitative analysis for determining the proportion

Table 2
Structural properties of the precursors.

Sample	Hydrotalcite phase (%)	2θ(003)	*d*(003)(Å)	*c*(Å)	2θ(110)	*d*(110)(Å)	*a*(Å)
Cu-100	0	–	–	–	–	–	–
Cu-70	57	6.75	13.08	39.24	–	–	–
Cu-50	86	6.75	13.08	39.24	63.03	1.47	2.94
Cu-30	100	6.75	13.08	39.24	62.70	1.48	2.96
Cu-0	100	6.22	14.20	42.60	62.49	1.49	2.98

of these crystalline phases in the precursor was performed. Rietveld refinement was not able to be run since there is no structural model of hydrotalcite with terephthalate in the open literature. Then, for the semi-quantitative analysis, the area under the main peak in both phases was calculated: hydrotalcite (at c.a. 6.0°) and the other phase in Cu-100 (at c.a. 8.8°). The percentage area of the first peak was related to the hydrotalcite phase content. The results (Table 2) indicate that Cu-50 has less impurity.

Furthermore, for the hydrotalcite phase with terephthalate as the compensation anion, the *a* and *c* parameters were calculated for each sample, as well as the *d*(003) and *d*(110) distances. The *d*(003) reflection corresponds to the interlayer distance and the *d*(110) to the distance between the metallic atoms [27]. The results are presented in Table 2. For Cu-70, *d*(110) was not calculated due to the low intensity and resolution of the corresponding peak. There is a significant difference in the *c* parameter between Cu-0 and the other samples, being greater for Cu-0. This parameter is related to the basal reflections (003), (006), (009) and (0012), concerning the planes that form the hydrotalcite layers [27]. In Fig. 1 (when compared with the precursor Cu-0) those peaks are slightly shifted to higher 2θ values. Newman et al [36] showed that different orientations of the terephthalate anion in the interlayer region of hydrotalcites are possible, and consequently, this affects the *c* parameter and the first four peaks of the XRD pattern. In our case, a slight inclination of the terephthalate occurred when copper was incorporated, probably due to the distortion of the copper octahedral caused by the Jahn-Teller effect.

Regarding the *a* parameter, there is almost no change, only a slight difference of 0.02 Å between Cu-0, Cu-30 and Cu-50. Ni^{2+} and Cu^{2+} have very similar ionic radius for octahedral coordination (0.69 and 0.73 Å), but Al^{3+} is smaller (0.53 Å) [37]. Therefore, the incorporation of Cu in Ni-Al hydrotalcite should not cause significant changes in the distance between metals, *d*(110), which has been also observed in other studies [38,39]. This small variation could indicate that more aluminum than expected effectively went into the lamellae of the hydrotalcite.

Fig. 2 shows the infrared spectra of the precursors. There are no bands between 2000 and 2500 cm^{-1}, and for this reason the 400-2000 cm^{-1} zone was amplified. An intense band in the region 3000-3700 cm^{-1} can be seen and is attributed to the O—H stretching, ν(OH), from the hydroxyl groups and also from the water molecules [38]. The relative intensity of this band is lower for the Cu-100 sample.

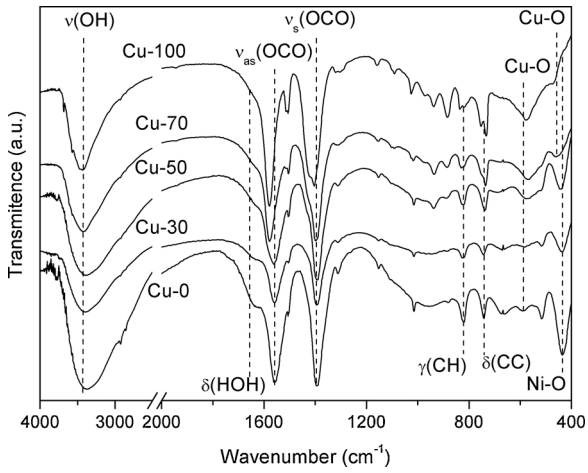

Fig. 2. Normalized infrared spectra of the precursors.

It probably occurs because the OH/TA ratio in copper-aluminum hydroxyterephthalate (the most likely phase found in Cu-100) is lower than the hydrotalcite phase (present in the other catalysts). This would be taking into account the theoretical formula for copper-aluminum hydroxyterephthalate as $Cu_xAl_{1-x}(OH)_{1+x}(TA)$ and for hydrotalcite $(Ni,Cu)_xAl_{1-x}(OH)_2(TA)_{x/2}.mH_2O$. All of the precursors have a water deformation band in 1642 cm^{-1}, which is attributed to the angular deformation of water molecules, δ (H—O—H) [40,41]. This band is less prominent in the Cu-100, and intensifies in the precursors that have higher proportion of hydrotalcite phase.

There are two bands with almost the same intensity at 1563 cm^{-1} and 1392 cm^{-1} attributed to the stretching vibration of the carboxylate ion (C═O) from the terephthalate anion. The weaker bands, at 742 and 820 cm^{-1}, also refer to the terephthalate anion (vibrations of benzene ring). Minor vibrations observed at 1502, 1308, 1154, 1104 and 516 cm^{-1} are assigned to C—H, C—O and C—C bonds [42].

The band at 435 cm^{-1} represents the vibration of the Ni—O bond stretching [43] and it is more intense for the precursor without copper (Cu-0). The characteristic bands from the Cu—O bond are localized at 585 and 450 cm^{-1} [44]. The band at 585 cm^{-1} is broader and more intense for the precursors with more copper content, as expected. The precursors with 70 and 100% of copper (related to the total divalent metals) have the bands of C═O displaced to 1580 cm^{-1}, possibly due to different interactions. Bands corresponding to ν_3 vibrational mode of CO_3, which would appear in about 1365 cm^{-1} [45] were not observed. This confirms the result found by XRD relative to absence of malachite phase ($Cu_2(OH)_2CO_3$).

The thermal analysis of the precursors (Fig. S2 of Supplementary Material) showed two main temperature regions. The first one, from room temperature up to ca. 200 °C, was identified as an endothermic event, which consists of a loss of water molecules adsorbed on the surface and water molecules in the interlayer space. As copper content increases these events tend to join due to lower hydrotalcite content (as observed by XRD) because there is less water coming from the interlayer space. For this region, Cu-0, Cu-30 and Cu-50 precursors lose 20% w/w, whereas Cu-70 and Cu-100 precursors lose 14 and 6%w/w, respectively. Thus, Cu-100 has less water than the other precursors, as previously observed in the infrared results.

In the second region (between 200 and 600 °C) there is basically one event for Cu-0 and Cu-30, which is attributed to the dehydroxylation of the layers and loss of terephthalate anions present in the interlayer region of hydrotalcite [42]. For the other catalysts, two events clearly appear in the 300–500 °C range, which seems to come from the metal-terephthalate phase (found in Cu100). For Cu-50 there is an additional event around 520 °C, which can be generated from the terephathalate decomposition in the hydrotalcite. Cu-100 has the highest mass loss in the second region, which means that it consists mainly of organic material, probably aluminum/copper hydroxyterephthalate.

A temperature of 600 °C was selected as the calcination temperature of all precursors, since the materials practically do not lose mass beyond this temperature.

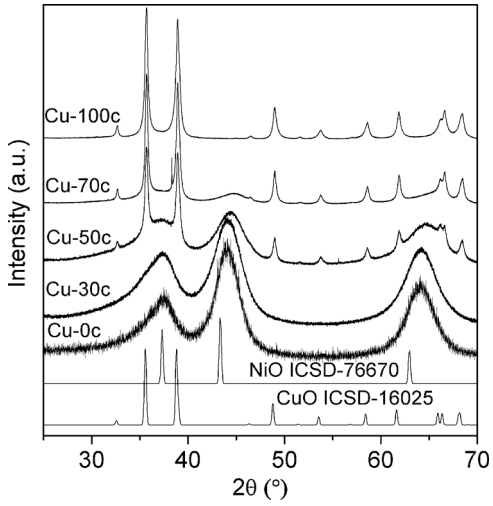

Fig. 3. XRD of the precursor calcined at 600 °C and patterns of NiO and CuO.

3.2. Catalysts

Fig. 3 shows the XRD of the catalysts and the NiO and CuO patterns. After calcination at 600 °C, the precursor Cu-0 and Cu-100 exhibited the NiO and the CuO crystalline phases, respectively. This means that there was a collapse of the precursor structure when calcination was carried out. The catalysts Cu-50c and Cu-70c showed a mixture of both crystalline phases, NiO and CuO. In Cu-30, CuO in crystalline form is not detected, meaning this phase can be considered totally amorphous.

The XRD of Cu-0c has the two last peaks (43.8 and 65°) of the NiO phase shifted to higher angles when compared with the pattern (43.3 and 63°). This behavior is due to the incorporation of aluminum into the NiO framework. The Al^{3+} radius (0.53 Å) is smaller than the Ni^{2+} (0.69 Å), then it reduces the unit cell parameters, as reported in the literature [46–48]. The remaining aluminum stayed as an amorphous phase, since evidence for the crystalline aluminum compound was not found.

In order to have a quantitative analysis of the crystalline phases in the two samples with CuO and NiO mixture (Cu-50 and Cu-70), the percentage of each phase was calculated by Rietveld refinement using GSAS software (see Table 3). CuO crystalline phase proportion increases with Cu content in the precursor. The change of phase percentage from Cu-50 to Cu-70 is higher than expected, indicating that a part of CuO is present as amorphous phase in Cu-50 and the same occurs with amorphous NiO in Cu-70.

The Fig. 4 shows the X-ray diffractograms of the catalysts obtained from the calcination of precursors at 900 °C. The peaks are more intense and better defined than the catalysts obtained after calcination of the precursors at 600 °C, which indicates greater crystallinity. The thermal treatment at higher temperature caused structural changes as Cu-Al and Ni-Al spinel formation, as well as increased the crystallinity of the phases already present in the catalysts, such as CuO and NiO oxides. With rising of temperature, the CuO phase, which was not so noticeable in the diffractogram of Cu-30c, now stands out. Only the diffractogram of Cu-0t does not exhibit high crystallinity, nevertheless, this is more crystalline than that of the corresponding catalyst calcined at 600 °C (Cu-0c).

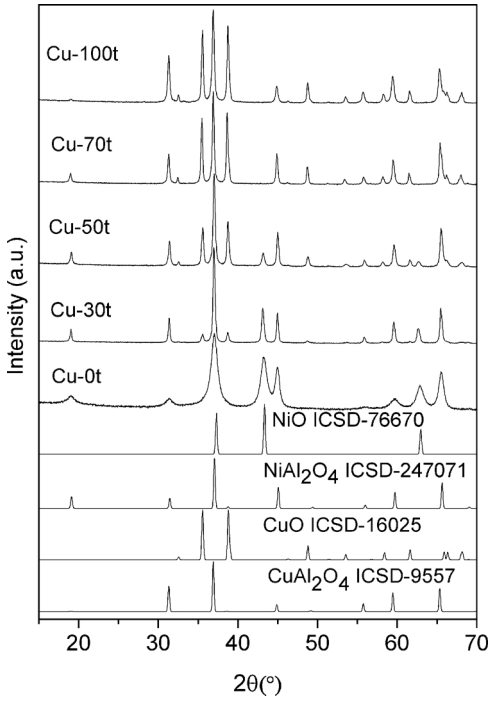

Fig. 4. XRD of the precursors calcined at 900 °C and patterns of NiO, CuO, $CuAl_2O_4$ and $NiAl_2O_4$.

As can be seen in Fig. 4, the spinel phases ($CuAl_2O_4$ and $NiAl_2O_4$) have their main peaks in almost the same position in 2θ, but with Rietveld refinement it was possible to determine the relative percentage of the crystalline phases. Powdercell software was used for the refinement. The results are displayed in Table 3. They show a logical trend of the NiO and CuO crystalline phases distribution (the more metal in the solid, the greater the amount of the crystalline metal oxide). The same trend for the aluminates phases is not present.

The catalyst Cu-70t does not exhibit crystalline NiO, indicating that

Table 3
Crystalline and textural properties of the catalysts.

Catalyst	Crystalline phases (%)				Average crystallite size (nm)[a]				Sg (m^2/g)
	CuO	NiO	$CuAl_2O_4$	$NiAl_2O_4$	CuO	NiO	$CuAl_2O_4$	$NiAl_2O_4$	
Cu-100c	100	0	0	0	19	–	–	–	83
Cu-70c	80	20	0	0	21	3.0	–	–	126
Cu-50c	20	80	0	0	15	2.8	–	–	165
Cu-30c	0	100	0	0	–	2.6	–	–	254
Cu-0c	0	100	0	0	–	2.7	–	–	289
Cu-100t	23	–	78	–	34	–	20	–	9
Cu-70t	15	–	42	43	41	–	13	43	7
Cu-50t	16	2	28	54	24	19	9	32	9
Cu-30t	3	10	32	55	35	19	18	34	3
Cu-0t	–	26	–	74	–	9	–	10	53

[a] The chosen peaks in the determination of the average crystallite size of the CuO and NiO phases were, respectively, 35.7 and 44°. For $NiAl_2O_4$ and $CuAl_2O_4$ was used the deconvolution of the peaks in 37°.

all nickel in the crystalline form is present as nickel aluminate. The catalysts with copper, for all intermediate compositions (y = 0.3, 0.5 and 0.7) presented higher nickel aluminate contents. Several authors claim that the $NiAl_2O_4$ phase is preferentially formed at high calcination temperatures (above 400 °C) and with longer aging time, which would favor the interaction of NiO with alumina [49,50]. In our case, the aluminates were formed at temperatures higher than 600 °C, suggesting a higher stability of the NiO phase in these catalysts. Another aspect to be highlighted is the relation between CuO and $CuAl_2O_4$. Note that this ratio presents a maximum point in the Cu-50 catalyst, indicating that the amount of copper oxide in this sample is proportionally higher compared to the others. Comparing the mass balance of metal in the precursor and in these catalysts it is possible to verify that all the aluminum is of the crystalline form, in the spinel structure.

The crystallite average sizes were also calculated and are presented in Table 3. It is interesting to compare the evolution of the CuO and NiO crystals sizes at the two calcination temperatures. Initially it can be noted that in the catalysts calcined at 600 °C, CuO crystals are much larger than those of NiO. When the materials are treated at higher temperatures, the crystals size increase, as expected, which is explained by the sintering phenomenon. After calcination at 900 °C, the CuO crystals double in size and the NiO crystals increase in a much larger proportion, from 3 to 7 times in relation to the sample calcined at 600 °C, but are still lower than CuO crystals. In samples calcined at 900 °C, it is also interesting to analyze the aluminate species. Note that the copper aluminate has crystals smaller than those of nickel and the sample Cu-50 t presented the smallest dimensions.

Table 3 shows the surface area of the catalysts, calculated from the nitrogen desorption data and from the BET model. It can be seen that the area has a linear tendency with Ni content (1-y). Since the alumina content is practically the same in the catalysts, the oxides in greater quantity will respond to variations in the area. Note that the increase in area follows the increase of the nickel content in the catalyst. These results are in agreement with that observed by XRD since the NiO crystallites are much smaller than those of CuO. Similar behavior was found by Souza et al. [51]

The catalysts in this study presented surface area higher than those reported in the literature, probably due to the use of terephthalate as the compensation anion. These catalysts, with copper and nickel (Cu-70c, Cu-50c and Cu-30c), had a surface area almost twice that of the Ni-Cu-Al materials obtained from carbonate-hydrotalcite. The same was observed for the nickel catalyst (Cu-0c), that had more than 1.5 times the surface area of that obtained using carbonate as the compensation anion [52]. All comparisons were made with catalysts with similar composition to ours. When results are compared with other compositions (metal/aluminum ratio), the differences reach higher values for Cu-Al [15,19] and Ni-Al [53].

The catalysts exhibited isotherm type IV with H3 hysteresis, according to the IUPAC classification, corresponding to mesoporous solids (Fig. S3(a) of Supplementary Material). The hysteresis loop is caused by the capillary condensation inside the pores [54].

The pore size distribution (Fig. S3(b) of the Supplementary Material) was obtained from the nitrogen adsorption isotherms using the BJH method [55]. The catalysts have pores of the mesoporous order (2–50 nm) and a small portion next to the microporous zone (around 3.5 nm), except Cu-100c. This behavior is in accordance with the literature for hydrotalcite-like materials [56,57]. As the nickel content increases, this portion also increases. The pore size distribution of the Cu-0c catalyst occurs in 3 different regions (around 3.5, 24.5 and 46.8 nm), while the Cu-30c catalyst has a similar distribution.

Table 3 also presents the BET surface area of the catalysts with thermal treatment at 900 °C. As expected, the surface area reduced significantly, caused by the sintering process. This is in agreement with results reported in the literature [15,16] for Cu-Al catalyst obtained from hydrotalcite materials. The thermal stability of Cu-0 catalyst is also noteworthy. Its area after 4 h at 900 °C reaches 53 m^2g^{-1} with a particle size of 9 nm. According to Dragoi et al. [58], nickel oxide surface enrichment with aluminum is responsible for the high thermal stability of this catalyst.

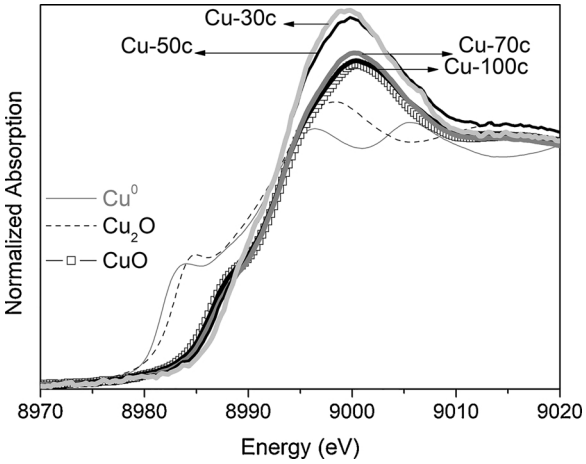

Fig. 5. Cu K-edge XANES spectra of the precursor calcined at 600 °C and the patterns Cu^0, Cu_2O and CuO.

Before starting the discussion on the redox properties of the catalysts, the normalized CuK-edge XANES spectra of the catalysts are presented in Fig. 5, collected at room temperature. The copper references in different oxidation states are also presented. These XANES spectra allow us to identify the initial oxidation state of copper species. It can be observed that all the catalysts have only Cu^{2+} species.

Fig. 6 presents the catalyst reduction profiles under H_2. The Cu-0c catalyst only starts to reduce at around 450 °C and presents a broad peak from 450 to 800 °C, attributed to reducible nickel species interacting with the alumina. The nickel reduction from a NiO prepared by decomposition of $Ni(NO_3)_2{\cdot}6H_2O$ at 500 °C occurs in the temperature range from 300 to 400 °C, considerably less than that observed in Fig. 6. According to the literature, nickel/alumina catalysts showed similar behavior, with reduction in the same temperature range, and were associated to the reduction of NiO interacting with alumina [48,58–60]. The higher dispersion of NiO on the catalyst probably promoted a stronger interaction, increasing the reduction temperature.

The Cu-100c catalyst is reduced in the range of 150 and 350 °C, lower than that observed for pure copper oxide (between 300 and 450 °C) [60]. Copper in presence of alumina is more easily reduced probably due to the lower interaction copper-alumina in this ex-hydrotalcite catalyst. Two reduction peaks, at 242 and 285 °C, can be

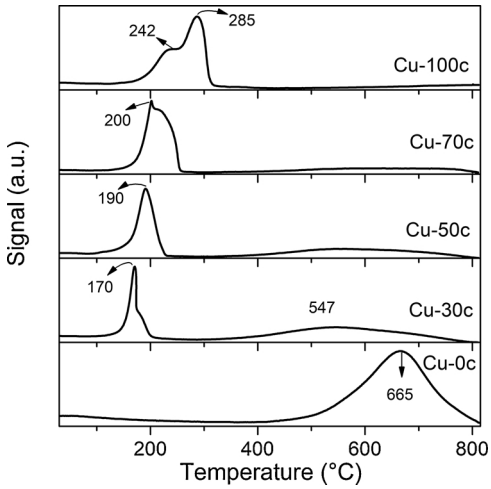

Fig. 6. H_2-TPR profiles of the precursor calcined at 600 °C, after pretreatment with He.

observed. The first peak is attributed to the more dispersed CuO species and the second is associated to CuO crystallites [61–63]. However, the possibility of reducing Cu^{2+} to Cu^{+} in the first peak, and Cu^{+} to Cu^{0} in the second one, can not be excluded, since the TPR peak deconvolution of Cu-100 profile (up to 350 °C, which corresponds to the reduction of copper) yields two peaks with nearly the same area. Muñoz et al. [15], studied CuAl catalysts and observed a reduction peak at 300 °C, attributed to the reduction of CuO from the "*bulk*" and one shoulder at 340 °C. This shoulder was attributed to the reduction of Cu_2O species. The presence of these species was confirmed by Raman analysis. This second peak could also correspond to the reduction of larger CuO particles [64,65].

The catalysts containing nickel and copper (Cu-30c, Cu-50c and Cu-70c) exhibit distinct reduction stages at low and high temperatures. The introduction of a second metal decreased the reduction temperature of the monometallic catalysts. The easier reduction of copper oxide over nickel is also clear. This behavior can be attributed to the molar free energy of reduction being lower for CuO ($-100.65\ kJ\ mol^{-1}$ at 25 °C) than for the NiO ($-12.31\ kJ\ mol^{-1}$ at 25 °C). The TPR profiles are similar to those reported in the literature for catalysts containing nickel and copper [51,52,58,59,66,67].

The catalyst containing 30% Cu shows two H_2 consumption peaks between 100 and 200 °C, attributed to the reduction of the more dispersed CuO and to CuO crystallites, respectively. This double peak moves to higher temperatures with increasing copper content. The first consumption peak decreases followed by an increasing of the second peak. This means that the dispersed copper oxide species decrease and have a higher interaction with the support. This behavior is in accordance with Wang et al. [62]. At the same time, the H_2 consumption peak at higher temperatures (between 450 and 800 °C), attributed to the reduction of nickel oxide, does not move while increasing copper content.

In any case, it is clear that the introduction of nickel into the copper catalyst shifted the reduction peaks to lower temperatures. According to Dragoi et al. [58], the presence of nickel and copper in the brucite like layers also improved the reducible properties of the catalysts. Thus, a synergic interaction between copper and nickel in close proximity to each other could justify this behavior. It is noteworthy that despite the observed interaction between copper and nickel, it seems that the corresponding oxides remain intact. There are no signals indicating a formation of a Ni-Cu alloy, as observed by Jha et al. [68]. Thus, the CuO reduction percentage presented in Table 4 refers to the consumption of hydrogen at low temperature (< 320 °C) and NiO at high temperature consumption (> 320 °C). Cu-70c presented the higher reduction of copper and nickel.

Taking into account the experimental error, the copper and nickel reduction percentage did not change very much in trimetallic catalysts. However, in the bimetallic (Cu-0c), nickel oxide reduction is lower than that of copper oxide. These variations are attributed to the lower free energy of CuO reduction compared to that of nickel, as previously mentioned.

Table 4
Reduction degree of the catalysts from the TPR experiments and temperatures and conversion data obtained from the *light-off* curves.

Catalyst	Reduction degree (%)		NO conversion		
	CuO	NiO	T50 (°C)[a]	T100 (°C)[b]	X_{500}[c]
Cu-100c	86	–	319	430	100
Cu-70c	94	62	306	430	100
Cu-50c	81	55	316	484	99
Cu-30c	89	54	327	479	98
Cu-0c	–	74	498	–	51

[a] Temperature at which 50% conversion is achieved.
[b] Temperature at which 100% conversion is achieved.
[c] Conversion at 500 °C.

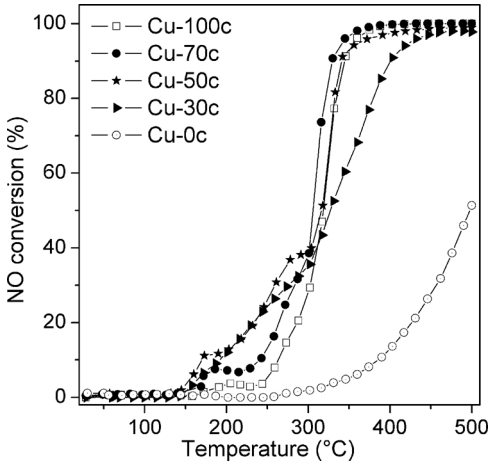

Fig. 7. NO conversion of the precursor calcined at 600 °C. Pretreatment: He at 300 °C for 1 h; flow rate of 225 mL min^{-1}. Reaction: Mixture NO and CO from room temperature up to 500 °C at 2 °C min^{-1}; flow rate of 225 mL min^{-1}.

Considering that the initial oxidation state of the catalysts was +2, as observed by XANES (Fig. 5) no complete reduction of metals was observed for all samples, even the TPR experiments being performed up to 800 °C. It is expected a final oxidation state of 0 for the metals, then a possible reduction during the pretreatment with an inert gas, as reported in the literature [42], could explain these results.

3.3. Catalytic tests

Fig. 7 presents the NO conversion light-off curves. The CO and NO conversions exhibited similar behaviors, for all catalysts (see Fig. S4 in the Supplementary Material). All catalysts, except Cu-0c, achieved near 100% conversion, thus the importance of copper in the NO reduction by CO reaction was clear. Cu-30c and Cu-50c catalysts were found to be the most active at lower temperatures (145–300 °C). This behavior is consistent with the results observed in the TPR experiments, which show that the catalysts are reduced at a lower temperature. However, this result is not very promising, as it will be discussed later.

The last three columns of Table 4 present, for each catalyst, T50 (temperature required for 50% conversion, here reported as the light-off temperature), T100 (temperature required for 100% conversion) and X_{500} (conversion reached at 500 °C). T50 changes slightly for copper catalysts, and there is no tendency to change with Cu content. Cu-100 and Cu-70 catalysts achieved 100% conversion at lower temperatures as observed by the T100 values. The Cu-0 catalyst is the least active.

The Cu-Ni catalysts show two smooth stages, the first between 150 and 300 °C (8% of NO conversion) and the second above 300 °C (35% of NO conversion). These events seem to be associated with the reaction mechanism. In the first stage, the Reaction (2) predominates and leads to the preferential formation of N_2O, which is confirmed by the high yield to nitrous oxide in this temperature range in comparison to N_2 formation (Fig. 8). In the second stage, above 300 °C, the N_2O yield decreases and that of N_2 increases exponentially up to approximately 320 °C. Thus, the high activity of Cu-30c and Cu-50c catalysts at low temperatures is associated with the N_2O formation, as presented in Fig. 8(b).

The maximum N_2O formation (Fig. 8(b)), as observed at well-defined intervals, coincides with the inflections found in NO conversion light-off curves. These inflections occur at lower temperatures (up to 300 °C) and appear to be related to the change of the reaction mechanism. The exception is the catalyst with 0% Cu, which forms N_2O at higher temperatures (289–500 °C) since it is active only above 350 °C.

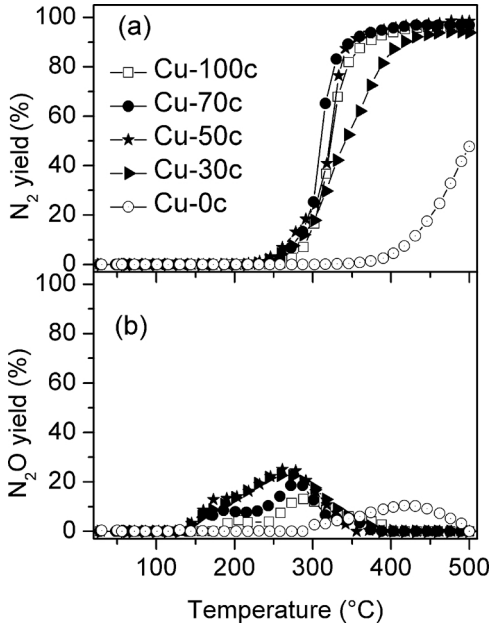

Fig. 8. N_2 yield (a) and N_2O yield (b) of the precursor calcined at 600 °C. Pretreatment: He at 300 °C for 1 h; flow rate of 225 mL min^{-1}. Reaction: Mixture NO and CO from room temperature up to 500 °C at 2 °C min^{-1}; flow rate of 225 mL min^{-1}.

According to the literature, the N_2O is formed at low temperature (< 250 °C) and its decomposition occurs at higher temperature (> 250 °C), as reported by Liu et al [69]. Patel et al [70] studied the activity of mesoporous alumina catalysts containing 4.5% of copper oxide. Their proposed mechanism is initiated by the adsorption of CO molecules in the catalyst surface. These adsorbed molecules connect to the oxygen from the CuO bulk, resulting in CO_2 adsorbed, which is subsequently desorbed. At this point, $–Cu^{\delta}+$ free species are formed (they represent reduced sites in the catalyst). Then, NO molecules in the gas phase adsorb at the $–Cu^{\delta+}$ and form the intermediate N–O $Cu^{\delta+}$, which combine with another NO molecule from the gas phase to form N_2O and regenerate the $–O–Cu^{\delta+}$ site. At higher Cu/Al ratios it was observed the average Cu–Cu distance decreases and a larger fraction of the Cu can form Cu–O–Cu bridges (dimers) [71]. The interaction between the dimers species and CO yields $\{Cu^{+}–[]–Cu^{+}\}$ species, where [] means oxygen vacancies, that are NO adsorption sites. Thus, the N_2O formation can be explained by the interaction among two NO molecules with $(Cu^{+}–[]–Cu^{+})$ species that results in the nitrous oxide formation and consequent recovery of the Cu–O–Cu species.

This reaction path is compatible with the results obtained in this work, since it relates N_2O formation with redox events of the copper species that are in high concentration at low temperatures.

Regarding the N_2O formation, the following sequence is observed: Cu-30c ≈ Cu-50c > Cu-70c > Cu-100c. Based on these results it is clear that the Ni increases the N_2O formation: higher copper content, higher N_2O formation. As discussed above, the presence of nickel anticipates the reduction process of the catalysts, promoting nitrous oxide formation. It is noteworthy that the sequence highlighted above is the same as that obtained when comparing the catalysts by the start of the reduction in TPR. Although Cu-0 presents less N_2O formation, this pollutant is formed at higher temperature ranges, which is undesirable since this temperature is close to those used in emission control systems.

The catalyst Cu-100c showed the lowest N_2O formation among copper catalysts (13% maximum at 287 °C). Thus, Cu-100c is one of the most active and the most selective for N_2. Considering that the catalytic activity is directly related to the redox properties of the catalyst [16], a monitoring of the oxidation state of copper throughout the reaction

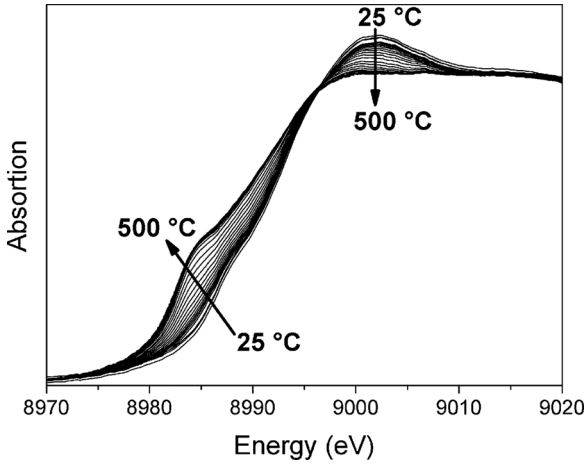

Fig. 9. Cu K-edge XANES spectra of Cu-100c obtained during in-situ experiments. Pretreatment: He at 150 °C for 20 min; flow rate of 40 mL min^{-1}. Reaction: Mixture NO and CO from room temperature up to 500 °C at 5 °C min^{-1}; flow rate of 50 mL min^{-1}. The arrows indicate the direction of the temperature increasing.

may contribute to the understanding the evolution of the different compounds during the reaction. So, XANES analysis of Cu-100 was performed under reaction conditions. It is noteworthy that any reduction process depends on the experimental conditions (flow rate, temperature, sample amount, temperature ramp, and so on) [72]. Figs. 9 and S5 of the Supplementary Material show the spectra obtained during the reaction. The oxidation state of copper is progressively changing (see Fig. 9), but from room temperature up to around 200 °C, the oxidation state of the catalyst remained constant, since the XANES spectra corresponds practically to the CuO pattern (see Fig. S5), i.e., mainly Cu^{2+} species were present. A continuous displacement of the absorption edge toward to the Cu_2O and Cu^0 above 200 °C can be observed, indicating that copper is reduced (or partially reduced) in these conditions.

Fig. 10 shows the copper species (Cu^{2+}, Cu^{+} and Cu^0) distribution throughout the reaction, obtained by means of the quantification of the XANES spectra. The catalyst presented 55% of Cu^{+} and 45% of Cu^0 species at 500 °C. At 23 °C, 83% Cu^{2+} and 17% of Cu^0 species were found. This means that the catalyst was reduced by 17% before the reaction, in the pretreatment stage. Note that a similar result was obtained in TPR tests (Cu-100c reduced only 86% after TPR up to 800 °C, started with a pretreatment at 500 °C under argon for 1 h). Thus, there is evidence that copper reduction is taking place during the

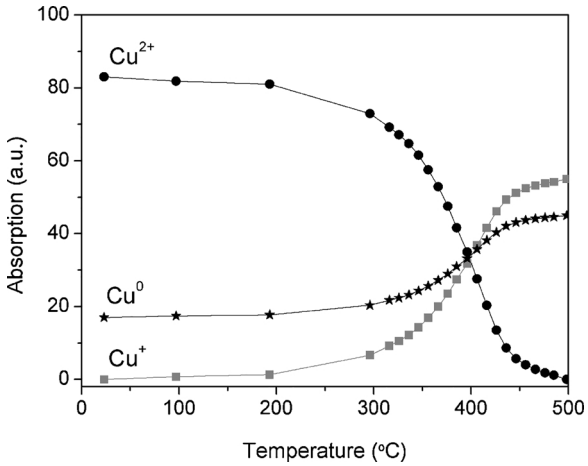

Fig. 10. Distribution of copper species throughout the reaction as a function of the temperature in of Cu-100c.

pretreatment stage under inert gas.

At the end of the reaction, Cu-100c does not present Cu^{2+} species. Cu^{+} species appear near to 200 °C, but from 300 to 500 °C they gradually increase. Corrêa et al. [16] studied a CuAl catalyst obtained from hydrotalcite type precursors containing carbonates (Cu:Al 50:50) and also verified Cu^{+} species around 300 °C using H_2-TPR accompanied by XANES. They observed that copper does not reduce directly from Cu^{2+} to Cu^{0} under the conditions studied. The copper reduction occurs in stages, since Cu^{+} was identified during the process.

According to the mass spectrometer data, collected during the XANES experiments using Cu-100c, 6% NO conversion is observed and the reaction starts at almost 350 °C, quite different from that observed previously (Fig. 7). It is noteworthy that the experimental conditions were different from those used in the conventional catalytic test. Two aspects may justify this difference: the sample amount and the type of reactor. The sample amount for the in-situ XANES experiment is much lower than that used in the catalytic test because the pellets were prepared with approximately 15 to 27 mg of the sample and 90 mg of the binder. In the catalytic test, 120 mg of catalyst were used. In addition, the reactors were different. While a fixed bed was used in the catalytic test, for in situ XANES reactor the pelletized catalysts were placed inside a tube, in a sample holder in which the reaction mixture could flow through the sample and also through the sides of that sample holder. This condition is quite different from the catalytic test where the mixture crossed the catalytic bed. Thus these XANES results cannot be compared exactly with the data from Fig. 7. In any case, the evolution of copper species throughout the reaction is clear, showing that the three copper species are present simultaneously. According to Vannice et al. [73] the activity of prereduced Cu/Al_2O_3 in CO oxidation is related to the presence of a superficial and thin layer of Cu_2O with oxygen vacancies or to interface sites between Cu_2O and Cu. Thus, the presence of reduced copper species seems to be important for the redox reactions as observed by XANES results.

In order to confirm the effect of the reduced species, some additional tests were performed changing the pretreatment gas, H_2 instead of He. The results are presented in Fig. 11. The improvement of the catalytic activity with the reduced catalyst is remarkable. Table 5 presents the light-off temperatures of the catalysts obtained from calcination of the precursor at 600 °C, using He and H_2 as pretreatment gases. T50 temperatures decrease significantly (see Table 5), possibly due to the greater availability of active species in the catalyst caused by the reducing treatment. Note that the catalysts containing nickel presented the greatest differences. It seems that nickel is only active in the reduced form in this reaction, but its reduction appears to be more difficult under the reaction conditions. With respect to the formation of nitrous oxide, there are changes on the N_2O yield curves when a pretreatment under H_2 is performed (see Fig. S6 in the Supplementary Material). There is less oscillation as well as a displacement for lower temperatures. Higher formation of nitrous oxide has also been observed and may be related to a probable increase of oxygen vacancies promoted by reduction of the catalysts. The previously observed trend was confirmed, i. e. increasing the nickel content increases the formation of nitrous oxide, according to the sequence from highest to lowest reducibility. It is worth mentioning the impact of the reducing pretreatment on Cu-0 (copper-free) catalyst in which the N_2O yield increased from approximately 10% to almost 40%. With these experiments, it was possible to confirm that Cu reduced species favor the performance of the catalyst for the NO by CO reduction.

Table 5
Comparison of performances of the calcined precursors.[a]

Precursor	600 °C (He)		600 °C (H_2)		900 °C (He)		ΔT_{50}[b]	ΔT_{50}[c]
	T50	N_2O yield	T50	N_2O yield	T50	N_2O yield		
Cu-100	318	13.0	278	8.3	289	25.2	−40	−29
Cu-70	306	18.5	213	12.2	322	10.8	−93	+16
Cu-50	316	25.0	214	17.9	314	13.6	−102	−2
Cu-30	327	22.7	242	26.4	437	8.1	−85	+110
Cu-0	498	10.4	298	36.5	–	5.2	−200	–

[a] Between parenthesis is the pretreatment gas, N_2O yield refers to maximum value.
[b] Difference of T50, considering different pretreatment gas and the same calcination temperature.
[c] Difference of T50, considering different calcination temperature and the same gas pretreatment.

Fig. 12 and Table 5 present the NO conversion and T50, respectively, of the precursors calcined at 900 °C. CO light-off curves are similar to the ones observed for the NO. The greatest impact was on the stability of activity at high temperatures (> 400 °C) when certain deactivation was observed. The catalyst Cu-30t presented the highest deactivation and Cu-0t only reaches a conversion of 30%. Cu-50t was the most thermally resistant, despite the drop in its surface area. It was also observed that Cu-100t (see Table 5) had a lower light-off temperature in comparison with Cu-100c, but it deactivated at temperatures higher than 400 °C. Muñoz et al. [15] studied catalysts obtained from the calcination of $CuAl\text{-}CO_3$ hydrotalcite-type materials and also found that after thermal deactivation the light-off temperatures decreased and the reducibility increased, despite the low surface areas. N_2 and N_2O yields for precursor calcined at 900 °C are presented in Fig. S7 in the Supplementary Material. N_2 formation occurs above 250 °C and

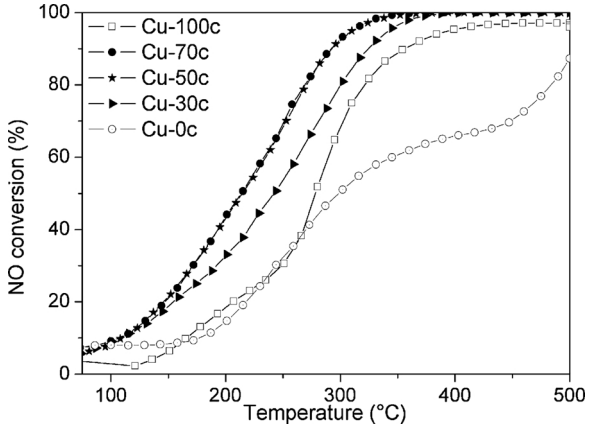

Fig. 11. Conversion of NO of the precursors calcined at 600 °C. Pretreatment: H_2 at 500 °C for 1 h; flow rate of 225 mL min^{-1}. Reaction: Mixture NO and CO from room temperature up to 500 °C at 2 °C min^{-1}; flow rate of 225 mL min^{-1}.

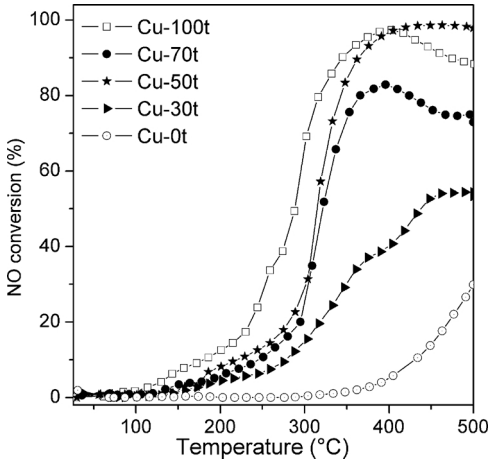

Fig. 12. Conversion of NO of the precursors calcined at 900 °C. Pretreatment: He at 300 °C for 1 h; flow rate of 225 mL min^{-1}. Reaction: Mixture NO and CO from room temperature up to 500 °C at 2 °C min^{-1}; flow rate of 225 mL min^{-1}.

predominates at temperatures higher than 300 °C. With regard to yield of N_2O, Cu-100t reaches the highest yield at N_2O, that is, 25% at 260 °C.

3.4. Effect of the composition of the precursor in the performance of the catalysts

As it was previously shown, different properties have been studied in the prepared Cu-Ni-Al materials (precursors and catalysts). The composition was close to that expected, but the structure was not always hydrotalcite in the precursors, as is the case of Cu-Al sample (without Ni). In all catalysts, the predominant crystalline phases were CuO and NiO, but in different proportions. For the catalysts calcined at 600 °C, an amount of non-crystalline aluminum species was also present, but for the samples calcined at 900 °C, practically all aluminum was in the crystalline form and, in addition to copper and nickel oxides, the presence of the phases $CuAl_2O_4$ and $NiAl_2O_4$ was also verified.

In the present work some results of the NO reduction by CO reaction are related to the catalysts properties, as composition, proportion of crystalline phase and surface area. In order to analyze the effect of Ni content in the performance of the catalyst, T50 and the maximum N_2O yield were listed as function of the fraction of Cu in the total divalent metals measured by XFR, for the catalysts calcined at 600 °C, 900 °C and calcined at 600 °C, but treated in H_2 atmosphere (see Table 5).

It is possible to see that the incorporation of nickel in low quantities did not cause a noticeable improvement in activity (light-off temperature) when the precursor is calcined at 600 °C and is not previously reduced. T50 increases when Ni is in higher quantities, which means that copper presence in higher contents gives better performance. The introduction of nickel in the Cu-100c catalyst also promote N_2O formation. However, the performance of the catalysts significantly change after pretreatment with hydrogen before the reaction. Cu-50c and Cu-70c have the lowest T50 what means that nickel has to be reduced to achieve its best performance in the presence of copper. Among Ni-containing catalysts, Cu-50c reached 100% N_2 selectivity at the lowest temperature (< 350 °C). For catalysts calcined at 900 °C, Cu-50t achieved 100% selectivity to N_2 at the lowest temperature (< 420 °C) and proved to be thermally stable. This good performance of the Cu-50 catalyst (precursor calcined at 600 and 900 °C) can be justified by some aspects observed throughout the work. It has a high surface area, the smallest CuO crystal size and presents the lowest percentage of copper aluminate when its precursor is calcined at 900 °C. Apparently, during pretreatment under He, it also reduces more than the other catalysts.

The long-term stability results performed with the better catalysts are present in Fig. S8 of the Supplementary Material. Once the desired temperature is reached, there is no loss of activity, i. e., there is no deactivation over time on stream. The drop in conversion observed in the catalysts calcined at 900 °C probably indicates that there are fewer surface sites available.

Regarding the effect of the hydrotalcite compensation anion in the reaction, a comparison shows that terephthalate has advantages over carbonate [16], even when prepared using the same metals, precipitating agents, and composition (x value). The light-off temperature using Cu-Al-CO_3 as precursor is 380 °C and with Cu-Al-TA is 319 °C. In spite of a pure hydrotalcite was not obtained using therephthalate, this precursor generates catalysts with surface areas much higher than those obtained using carbonate [15,16]. The importance of the precursor in the final catalytic performance is also clear. Despite the precursor being a previous step of the catalyst and despite the final catalyst consisting of the CuO crystalline phase and amorphous aluminum species, the difference in the catalytic behavior is clear, in both catalysts. Indeed, XANES showed that a partial reduction of copper was possible even in an inert atmosphere, outlining the reactivity of Cu-Al-TA.

Finally, graphs comparing the performance of different noble metal catalyst supported in ceria-zirconia (Pd/CZ, Pt/CZ, Rh/CZ) with our Cu-Ni-Al catalyst were made (Fig. S9 of Supplementary Material). Catalytic tests of these metal noble materials had been carried out in our lab, so these were run under the same conditions of the catalyst reported in this paper. The results show that noble metal catalysts stand out in terms of NO conversion, especially rhodium and palladium, being Rh one, similar to our Cu-Ni-Al catalyst. It is also possible to observe that the yield to nitrous oxide with mixed oxide derived from Cu-Ni-Al hydrotalcite presents a different behavior, generating less N_2O and conversions that reach 100% around 350 °C.

4. Conclusions

The precursor synthesis method was appropriate for the incorporation of all metals in the desired proportion. Obtention of a pure hydrotalcite phase was possible for 100% and 70% Ni (Cu-0 and Cu-30).

At room temperature, all the catalysts have only Cu^{2+} species. Copper-reduced species appear even during thermal pretreatment with inert gas, as well as throughout the reaction of NO by CO.

The performance of the copper-nickel catalysts depends significantly on the mixed oxide preparation method as well as the oxidation state of copper and nickel. Reduced species have shown better catalytic performance. These catalysts reached 100% N_2 selectivity at the lower temperature than the copper catalysts.

The calcination temperature of the precursors strongly affected the characteristics of the catalysts. The catalysts obtained by the calcination of the precursor at 600 °C formed the NiO and CuO crystalline phases, but at 900 °C, additionally, spinel phases appear. At 600 °C the surface area was one order higher than those at 900 °C. A linear relation was exhibited between the surface area and Ni percentage.

Cu-50 proved to be the best catalyst because of its good textural and structural characteristics, good reducibility, and high thermal and chemical stability. Furthermore, there was no deactivation over time on stream as observed by the long-term stability test.

The precursor influence is clear. Terephthalate as compensation anion has advantages over carbonate when prepared using the same metals, precipitating agents, and composition (x value): higher surface areas and higher activities.

The performance of the Cu-50 catalyst showed similar performance to that of a Rh/CZ catalyst (CZ: CeO_2-ZrO_2) but with the advantage of presenting a much lower N_2O yield.

Acknowledgments

We thank to FAPERJ [grant number 111.063/2013] and CNPq [grant number 484714/20139] by the financial support of this work. Daniel Lopes would like to thank CAPES for the scholarship awarded. The authors would like to thank the Laboratório Nacional de Luz Síncroton (Campinas, Brazil) for project approval and financial support during the DXAS (project 20150337) and XPD (project 201pre60235) measurements. Also, we thank to the Laboratório Multiusuário (IQ/UFRJ) for XRD analysis, LABCATH (IQ/UFRJ) for the availability of the FTIR spectrometer and CETEM for the XFR analysis.

Appendix A. Supplementary data

Supplementary material related to this article can be found, in the online version, at doi:https://doi.org/10.1016/j.apcatb.2018.06.007.

References

[1] G.L. Haller, New Insights on the Mechanism of the NO Reduction With CO Over Alumina-Supported Copper Catalysts, (1995), pp. 16380–16382.
[2] Y. Nagai, K. Dohmae, Y.F. Nishimura, H. Kato, H. Hirata, N. Takahashi, Operando XAFS study of catalytic NO reduction over Cu/CeO_2: the effect of copper-ceria interaction under periodic operation, Phys. Chem. Chem. Phys. 15 (2013) 8461–8465.
[3] X. Yao, F. Gao, Q. Yu, L. Qi, C. Tang, L. Dong, Y. Chen, NO reduction by CO over $CuO–CeO_2$ catalysts: effect of preparation methods, Catal. Sci. Technol. 3 (2013)

1355.
[4] Y. Hu, L. Dong, M. Shen, D. Liu, J. Wang, W. Ding, Y. Chen, Influence of supports on the activities of copper oxide species in the low-temperature NO + CO reaction, Appl. Catal. B Environ. 31 (2001) 61–69.
[5] L.A. Flores-Sanchez, J.M. Quintana-Melgoza, A. Olivas, M. Avalos-Borja, Reduction of nitric oxide by carbon monoxide over NiO, CuO, and ZnO catalysts, React. Kinet. Mech. Catal. 114 (2015) 597–609.
[6] C. Ge, L. Liu, X. Yao, C. Tang, F. Gao, L. Dong, Treatment induced remarkable enhancement of low-temperature activity and selectivity of copper-based catalysts for NO reduction, Catal. Sci. Technol. 3 (2013) 1547.
[7] Y. Kong, Y. Zhang, X. Wa, J. Wang, H. Wan, L. Dong, Q. Yan, Catalytic performance of Cu-MCM41 with high copper content for NO reduction by CO, Stud. Surf. Sci. Catal. 165 (2007) 749–753.
[8] R. Zhang, A. Villanueva, H. Alamdari, S. Kaliaguine, Reduction of NO by CO over nanoscale $LaCo_{1-x}Cu_xO_3$ and $LaMn_{1-x}Cu_xO_3$ perovskites, J. Mol. Catal. 258 (2006) 22–34.
[9] C. Drouet, P. Alphonse, A. Rousset, New spinel materials for catalytic NO–CO reaction: nonstoichiometric nickel–copper manganites, Appl. Catal. B Environ. 33 (2001) 35–43.
[10] F. Cavani, F. Trifirò, A. Vaccari, Hydrotalcite-type anionic clays: preparation, properties and applications, Catal. Today 11 (1991) 173–301.
[11] T. Machej, E.M. Serwicka, M. Zimowska, R. Dula, A. Michalik-Zym, B. Napruszewska, W. Rojek, R. Socha, Cu/Mn-based mixed oxides derived from hydrotalcite-like precursors as catalysts for methane combustion, Appl. Catal. A Gen. 474 (2014) 87–94.
[12] E. Genty, J. Brunet, R. Pequeux, S. Capelle, S. Siffert, R. Cousin, Effect of Ce substituted hydrotalcite-derived mixed oxides on total catalytic oxidation of air pollutant, Mater. Today Proc. 3 (2016) 277–281.
[13] J. Pérez-Ramírez, S. Abelló, N.M. Van Der Pers, Influence of the divalent cation on the thermal activation and reconstruction of hydrotalcite-like compounds, J. Phys. Chem. C 111 (2007) 3642–3650.
[14] J. He, M. Wei, B. Li, Y. Kang, D.G. Evans, X. Duan, Layered Double Hydroxides, Springer-Verlag, Berlin/Heidelberg, 2006.
[15] V. Muñoz, F.M. Zotin, L.A. Palacio, Copper–aluminum hydrotalcite type precursors for NOx abatement, Catal. Today 250 (2014) 173–179.
[16] C.L. Corrêa, Y.E. Licea, L.A. Palacio, F.M. Zotin, Effect of composition and thermal treatment in catalysts derived from Cu-Al hydrotalcites-like compounds in the NO reduction by CO, Catal. Today 289 (2017) 133–142.
[17] K. Yan, J. Liao, X. Wu, X. Xie, Facile synthesis of eco-friendly cu-hydrotalcite catalysts for highly selective synthesis of furfural diethyl acetal and benzoin ethyl ether, Adv. Mater. Lett. 4 (2013) 702–707.
[18] Y. Lwin, M.A. Yarmo, Z. Yaakob, A.B. Mohamad, W. Ramli Wan Daud, Synthesis and characterization of Cu–Al layered double hydroxides, Mater. Res. Bull. 36 (2001) 193–198.
[19] S. Velu, C. Swamy, Selective c-alkylation of phenol with methanol over catalysts derived from copper-aluminium hydrotalcite-like compounds, Appl. Catal. A Gen. 145 (1996) 141–153.
[20] S. Gago, M. Pillinger, T.M. Santos, I.S. Gonçalves, Zn-Al Layered double hydroxide pillared by different dicarboxylate anions, Ceram. - Silikaty 48 (2004) 155–158.
[21] S. Arias, J.G. Eon, R.A. San Gil, Y.E. Licea, L.A. Palacio, A.C. Faro, Synthesis and characterization of terephthalate-intercalated NiAl layered double hydroxides with high Al content, Dalton. Trans. 42 (2013) 2084–2093.
[22] T. Coelho, R. Micha, S. Arias, Y.E. Licea, L.A. Palacio, A.C. Faro, Influence of the Mg^{2+} or Mn^{2+} contents on the structure of NiMnAl and CoMgAl hydrotalcite materials with high aluminum contents, Catal. Today 250 (2015) 87–94.
[23] M. Meyn, K. Beneke, G. Lagaly, Anion-exchange reactions of layered double hydroxides, Inorg. Chem. 29 (1990) 5201–5207.
[24] E. Crepaldi, J. Tronto, L. Cardoso, J. Valim, Sorption of terephthalate anions by calcined and uncalcined hydrotalcite-like compounds, colloids surfaces A physicochem, Eng. Asp. 211 (2002) 103–114.
[25] G.L. Bauerle, L.L.C. Sorensen, K. Nobe, Nitric oxide reduction on copper-nickel catalysts, Prod. R&D 13 (1974) 61–64.
[26] G. Perin, J. Fabro, M. Guiotto, Q. Xin, M.M. Natile, P. Cool, P. Canu, A. Glisenti, Cu@LaNiO3based nanocomposites in TWC applications, Appl. Catal. B Environ. 209 (2017) 214–227.
[27] D.G. Evans, C.T. Slade, Structural aspects of layered double hydroxides, Struct. Bond. 119 (2006) 1–87.
[28] G. Kraus, W. Nolze, PowderCell for Windows, (1999).
[29] A.C. Larson, R.B. Von Dreele, General Structure Analysis System (GSAS), Los Alamos (2000).
[30] K.P. Scherrer, Bestimmung der grosse und der inneren struktur von kolloidteilchen mittels rontgenstrahlen, Math.-Phys. (1918) 98–100.
[31] A. Gaur, B.D. Shrivastava, A comparative study of the methods of speciation using X-ray absorption fine, Acta Phys. Pol. A 121 (2012) 647–652.
[32] A. Gaur, B.D. Shrivastava, S.K. Joshi, Copper K-edge XANES of Cu(I) and Cu(II) oxide mixtures, J. Phys. Conf. Ser. 190 (2009) 1–4.
[33] M. Shacham, M.B. Cutlip, M. Elly, Polymath 5.0, (2000).
[34] S.P. Newman, W. Jones, Synthesis, characterization and applications of layered double hydroxides containing organic guests, New J. Chem. (1998) 105–115.
[35] T. Loiseau, C. Serre, C. Huguenard, G. Fink, F. Taulelle, M. Henry, T. Bataille, G. Férey, A rationale for the large breathing of the porous aluminum terephthalate (MIL-53) upon hydration, Chemistry 10 (2004) 1373–1382.
[36] S.P. Newman, S.J. Williams, P.V. Coveney, W. Jones, Interlayer arrangement of hydrated MgAl layered double hydroxides containing guest terephthalate anions: comparison of simulation and measurement, J. Phys. Chem. B 102 (1998) 6710–6719.
[37] R.D. Shannon, Revised effective ionic radii and systematic studies of interatomie distances in halides and chaleogenides, Acta Cryst. A32 (1976) 751–767.
[38] G. Carja, R. Nakamura, T. Aida, H. Niiyama, Textural properties of layered double hydroxides: effect of magnesium substitution by copper or iron, Microporous Mesoporous Mater. 47 (2001) 275–284.
[39] M. Crivello, C. Pérez, E. Herrero, G. Ghione, S. Casuscelli, E. Rodríguez-Castellón, Characterization of Al-Cu and Al-Cu-Mg mixed oxides and their catalytic activity in dehydrogenation of 2-octanol, Catal. Today 107–108 (2005) 215–222.
[40] F. Kooli, I.C. Chisem, M. Vucelic, W. Jones, Synthesis and properties of terephthalate and benzoate intercalates of Mg-Al layered double hydroxides possessing varying layer charge, Chem. Mater. 4756 (1996) 1969–1977.
[41] J. Das, K.M. Parida, Heteropoly acid intercalated Zn/Al HTlc as efficient catalyst for esterification of acetic acid using n-butanol, J. Mol. Catal. A Chem. 264 (2007) 248–254.
[42] Z.P. Xu, H.C. Zeng, Decomposition processes of organic-anion-pillared clays $Co_aMg_bAl(OH)_c(TA)_d.nH_2O$, Technol. Phys. Chem. B (2000) 10206–10214.
[43] M. Jitianu, Thermal behaviour of hydrotalcite-like compounds: study of the resulting oxidic forms, Int. J. Inorg. Mater. 2 (2000) 287–300.
[44] M.A. Ocaña, Síntesis de hidrotalcitas y materiales derivados: aplicación en Catálisis Básica, (2005).
[45] J.T. Kloprogge, D. Wharton, L. Hickey, R.L. Frost, Infrared and Raman study of interlayer anions CO_3 in Mg / Al- hydrotalcite, Am. Miner. 87 (2002) 623–629.
[46] V. Rives, S. Kannan, Layered double hydroxides with the hydrotalcite-type structure containing Cu^{2+}, Ni^{2+} and Al^{3+}, J. Mater. Chem. 10 (2000) 489–495.
[47] F. Kovanda, T. Rojka, P. Bezdička, K. Jirátová, L. Obalová, K. Pacultová, Z. Bastl, T. Grygar, Effect of hydrothermal treatment on properties of Ni-Al layered double hydroxides and related mixed oxides, J. Solid State Chem. 182 (2009) 27–36.
[48] E.M. Fuentes, A. Faro, T. Silva, J.M. Assaf, M.C. Rangel, A comparison between copper and nickel-based catalysts obtained from hydrotalcite-like precursors for WGSR, Catal. Today 171 (2011) 290–296.
[49] J.A. Peña, J. Herguido, C. Guimon, A. Monzón, J. Santamaría, Hydrogenation of acetylene over $Ni/NiAl_2O_4$ catalyst: characterization, coking, and reaction studies, J. Catal. 159 (1996) 313–322.
[50] Y. Cesteros, P. Salagre, F. Medina, J.E. Sueiras, Preparation and characterization of several high-area $NiAl_2O_4$ spinels. Study of their reducibility, Chem. Mater. 12 (2000) 331–335.
[51] G. De Souza, N.M. Balzaretti, N.R. Marcílio, O.W. Perez-Lopez, Decomposition of ethanol over Ni-Al catalysts: effect of copper addition, Procedia Eng. 42 (2012) 335–345.
[52] J. Ashok, M. Subrahmanyam, A. Venugopal, Hydrotalcite structure derived Ni-Cu-Al catalysts for the production of H_2 by CH_4 decomposition, Int. J. Hydrogen Energy 33 (2008) 2704–2713.
[53] J.A. Valverde, A. Echavarría, M.F. Ribeiro, L.A. Palacio, J.G. Eon, Decavanadate-intercalated Ni-Al hydrotalcites as precursors of mixed oxides for the oxidative dehydrogenation of propane, Catal. Today 192 (2012) 36–43.
[54] K.S.W. Sing, D.H. Everett, R.A.W. Haul, L. Moscou, L.A. Pierotti, J. Rouquerol, T. Siemieniewska, Reporting physisorption data for gas/soils systems with special reference to the determination of surface area and porosity, Pure Appl. Chem. 57 (1985) 603–619.
[55] L.G. Joyner, E.P. Barrett, R. Skold, The determination of Pore volume and Area distributions in porous substances. II. Comparison between nitrogen isotherm and mercury porosimeter methods, J. Am. Ceram. Soc. 73 (1951) 3155–3158.
[56] P. Kuśtrowski, L. Chmielarz, E. Bozek, M. Sawalha, F. Roessner, Acidity and basicity of hydrotalcite derived mixed Mg-Al oxides studied by test reaction of MBOH conversion and temperature programmed desorption of NH3 and CO2, Mater. Res. Bull. 39 (2004) 263–281.
[57] B. Dudek, P. Kuśtrowski, A. Bialas, P. Natkański, Z. Piwowarska, L. Chmielarz, M. Kozak, M. Michalik, Influence of textural and structural properties of Mg-Al and Mg-Zn-Al containing hydrotalcite derived oxides on Cr(VI) adsorption capacity, Mater. Chem. Phys. 132 (2012) 929–936.
[58] B. Dragoi, A. Ungureanu, A. Chirieac, C. Ciotonea, C. Rudolf, S. Royer, E. Dumitriu, Structural and catalytic properties of mono- and bimetallic nickel-copper nanoparticles derived from MgNi(Cu)Al-LDHs under reductive conditions, Appl. Catal. A Gen. 504 (2015) 92–102.
[59] D. Li, M. Koike, J. Chen, Y. Nakagawa, K. Tomishige, Preparation of Ni-Cu/Mg/Al catalysts from hydrotalcite-like compounds for hydrogen production by steam reforming of biomass tar, Int. J. Hydrogen Energy 39 (2014) 10959–10970.
[60] S. Robertson, D. McNicol, J. Baas, S. Kloet, Determination of reducibility and identification alloying in copper-nickel-on-silica catalysts reduction of by temperature-programmed reduction, J. Catal. 431 (1975) 424–431.
[61] W.-P. Dow, Y.-P. Wang, T.-J. Huang, Yttria-stabilized zirconia supported copper oxide catalyst, J. Catal. 160 (1996) 155–170.
[62] W. Dow, Y. Wang, T. Huang, TPR and XRD studies of yttria-doped ceria/γ-alumina-supported copper oxide catalyst, Appl. Catal. A Gen. 190 (2000) 25–34.
[63] V. Thyssen, T. Maia, E. Assaf, Cu and Ni catalysts supported on γ-Al_2O_3 and SiO_2 assessed in glycerol steam reforming reaction, J. Braz. Chem. Soc. 26 (2015) 22–31.
[64] B. Bridier, N. López, J. Pérez-Ramírez, Partial hydrogenation of propyne over copper-based catalysts and comparison with nickel-based analogues, J. Catal. 269 (2010) 80–92.
[65] J.M. Dumas, C. Geron, A. Kribii, J. Barbier, Preparation of supported copper catalysts. II. Reduction of copper/alumina catalysts, Appl. Catal. 47 (1989) L9–L15.
[66] P. Tuza, R. Manfro, N. Ribeiro, M. Souza, Production of renewable hydrogen by aqueous-phase reforming of glycerol over Ni-Cu catalysts derived from hydrotalcite precursors, Prog. Sustain. Energy Technol. Gen. Renew. Energy 1 (2014) 413–426.
[67] H. Zhu, M. Zhou, Z. Zeng, G. Xiao, R. Xiao, Selective hydrogenation of furfural to cyclopentanone over Cu-Ni-Al hydrotalcite-based catalysts, Korean J. Chem. Eng.

31 (2014) 593–597.
[68] A. Jha, D. Jeong, J. Shim, W. Jang, Y. Lee, C.V. Rode, H. Roh, Hydrogen production by the water-gas shift reaction using CuNi/Fe_2O_3 catalyst, Catal. Sci. Technol. 5 (2015) 2752–2760.
[69] L. Yu, W. Xue-Zhong, Y. Xiang-Guang, W. Yue, Catalytic reduction of NOx by CO on hydrotalcites-derived mixed oxides CoAlM and MgAlM (M = Cr, Mn, Fe, Co, Ni, Cu), Chin. J. Chem. 17 (2010) 599–608.
[70] A. Patel, P. Shukla, J. Chen, T.E. Rufford, S. Wang, V. Rudolph, Z. Zhu, Structural sensitivity of mesoporous alumina for copper catalyst loading used for NO reduction in presence of CO, Chem. Eng. Res. Des. 101 (2015) 27–43.
[71] P. Da Costa, B. Modén, G.D. Meitzner, D.K. Lee, E. Iglesia, Spectroscopic and chemical characterization of active and inactive Cu species in NO decomposition catalysts based on Cu-ZSM5, Phys. Chem. Chem. Phys. 4 (2002) 4590–4601.
[72] Y.J. Huang, H.P. Wang, M.C. Hsiao, C.C. Tai, H.L. Huang, S.H. Liu, Speciation of copper in micropores, Water Air Soil Pollut. 153 (2004) 187–194.
[73] C.K.A. Vannice, CO oxidation over Pd and Cu catalysts, J. Catal. 50 (1991) 36–50.